

New approach for modelling distributed MEMS transmission lines

K. Topalli, M. Unlu, S. Demir, O. Aydin Civi, S. Koc and T. Akin

Abstract: The paper presents a new and more accurate model for the distributed MEMS transmission line (DMTL) structures. In this new model, the MEMS bridges that are used as the loading elements of the DMTL structures are represented as low-impedance transmission lines, rather than a lumped *CLR* circuit. The model also includes *LC* networks at the transition points from the MEMS bridges to the unloaded parts of the DMTL, which are simply high-impedance transmission lines. These *LC* networks are employed to model the effects of the impedance discontinuities. The accuracy of the model is verified with simulations and measurements in the range 1–20 GHz on various DMTL structures that are fabricated with an RF MEMS process based on electroforming on a glass substrate. The measurement results of the fabricated devices are in good agreement with the model with an error less than 5%. It is shown that this new model provides better agreement than the conventional method for the DMTL structures with a bridge width larger than 50 μm .

1 Introduction

Distributed MEMS transmission lines (DMTLs) are used in implementation of phase shifters [1–4], resonators [5] and filters [6], which are the key components in phased arrays, radars, wireless communication systems and measurement instrumentation. The implementation of DMTLs employs the idea of periodically loading a high-impedance coplanar waveguide (CPW) with reactive loading elements. Generally, the loading elements are tunable RF MEMS bridges, forming a transmission line with adjustable parameters [1–4]. Accurate modelling of DMTL structures is crucial in order to reduce the computational and implementation time. The main approach for modelling of DMTL structures is based on the modelling of the MEMS bridge as a lumped-series *CLR* circuit [1]. However, the *CLR* model deviates from the DMTL characteristics when MEMS bridge dimensions are increased, because the lumped element assumption is not valid for the DMTL structures with bridge widths larger than 50 μm .

This paper presents a new approach for modelling a DMTL structure, where the MEMS bridges in the DMTL structure are modelled with low-impedance transmission lines and two *LC* networks that account for the discontinuity effects [7, 8]. Simulations and measurement results of fabricated devices in 1–20 GHz band verify that this new model provides a good agreement for the DMTL structures, even with bridge widths larger than 50 μm .

2 Limitations of previous DMTL model

Modelling of a unit cell of a loaded line structure is essential to reduce computational time in simulating electrically long structures. Figure 1 shows the general view of a DMTL structure and existing model [2], which is composed of high-impedance transmission lines representing the unloaded CPW line and the *CLR* impedance to model the bridge in between two high-impedance transmission lines. In this

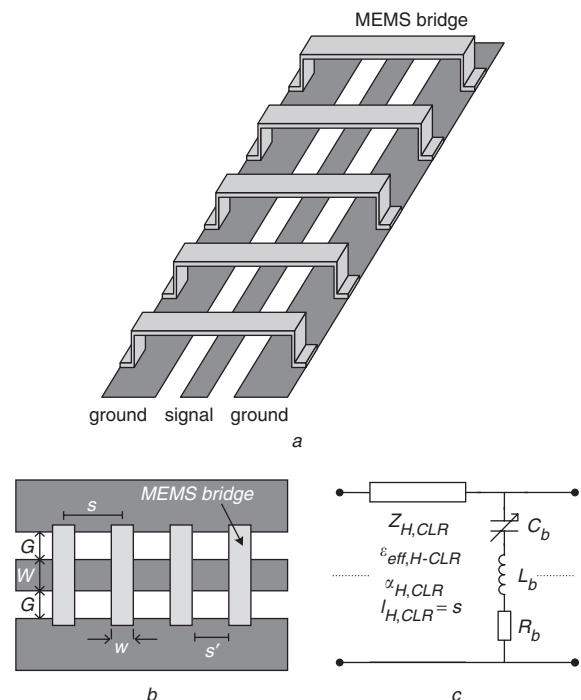


Fig. 1 General view of DMTL structure and existing model
a General view of a DMTL structure
b Top view of a DMTL structure
c Lumped-element *CLR* model of the unit section of DMTL [1]

© IEE, 2006

IEE Proceedings online no. 20050098

doi:10.1049/ip-map:20050098

Paper first received 29th April and in revised form 26th September 2005

The authors are with the Department of Electrical and Electronics Engineering, Middle East Technical University, Ankara, Turkey

E-mail: ozlem@metu.edu.tr

approach, an EM-based or a measurement result is fitted to the *CLR* model using optimisation tools, where C , L and R are free variables by minimising the least square error. To date, the model has been used successfully to describe the operation of DMTL structures with electrically short bridge widths. However, this model cannot provide satisfactory results for structures with relatively large bridge structures (i.e. when the bridge width is larger than $50\mu\text{m}$), which is necessary to obtain more phase shift for phase shifter applications. Table 1 describes two DMTL structures as case studies, where it is shown that the *CLR* model provided in [2] works for case I with short bridge width, but not for case II with relatively long bridge width. Consider-

Table 1: Physical description of DMTL structures on quartz ($\epsilon_r = 3.8$, $h = 500\mu\text{m}$) investigated for the validity of the *CLR* model

Parameter, μm	Case I	Case II
W	100	100
G	100	100
w	35	100
s	197	262
s'	162	162
h	1.2	1.2

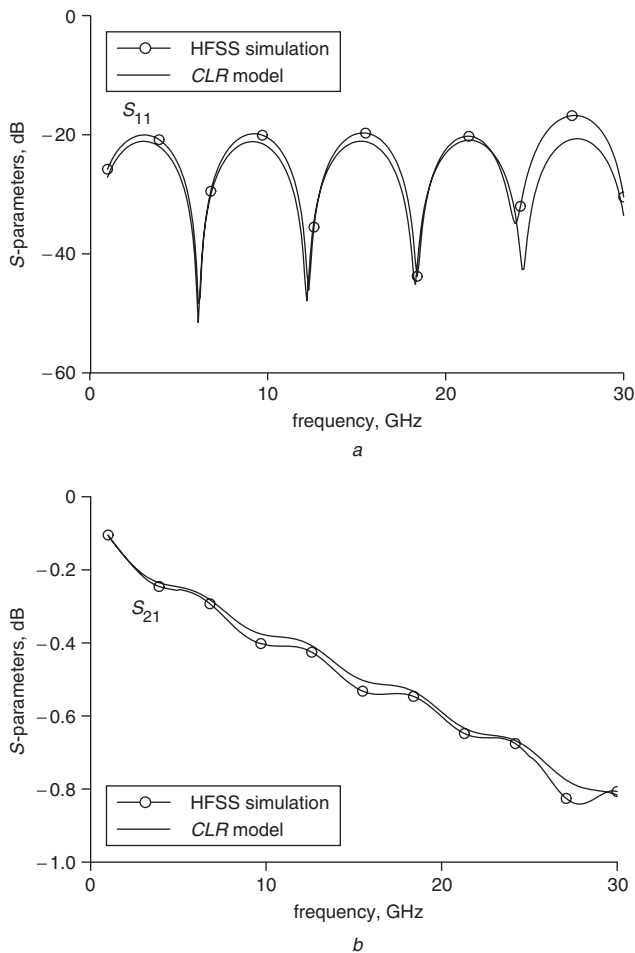


Fig. 2 *S*-parameter results for DMTL structure with $35\mu\text{m}$ bridge width as described in case I in Table 1

a Reflection characteristics
b Transmission characteristics

This example shows that a good agreement between the model and simulation can be achieved with the *CLR* model given in [2] when the bridge width is $35\mu\text{m}$

ing these cases, a 10 bridge section in Ansoft HFSSv9.2 is simulated, and its *S*-parameters are cascaded in Agilent ADS 2003 to obtain EM simulation result for a DMTL structure with 40 bridges.

Figure 2 shows *S*-parameter results for the DMTL structure with a $35\mu\text{m}$ bridge width as described in case I in Table 1. This example shows that a good agreement between the model and simulation can be achieved with the *CLR* model given in [2] when the bridge width is $35\mu\text{m}$. However, Fig. 3 shows that a satisfactory agreement between the model and simulation cannot be achieved with the model in [2] when the bridge width is $100\mu\text{m}$ as described in case II in Table 1. Table 2 lists the extracted

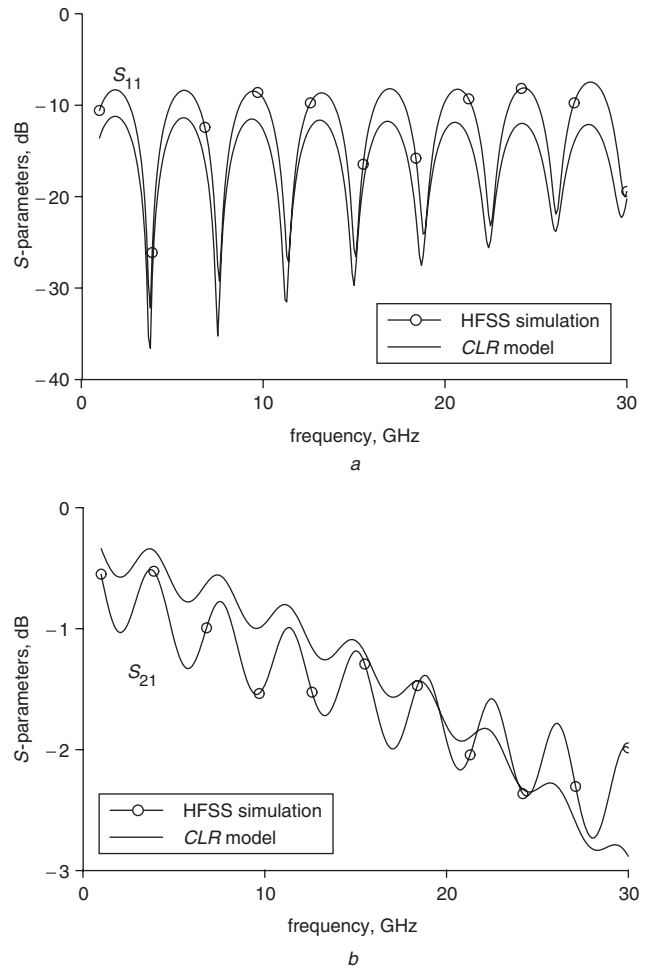


Fig. 3 *S*-parameter results for DMTL structure with $100\mu\text{m}$ bridge width as described in case II in Table 1

a Reflection characteristics
b Transmission characteristics

This example shows that the agreement between the model and simulation is not satisfactory with the *CLR* model given in [2] when the bridge width is $100\mu\text{m}$

Table 2: Evaluated parameters of the *CLR* model for the DMTL structure with dimensions in Table 1

Parameter	Case I	Case II
C_b	32.6 fF	74.1 fF
L_b	20 pH	20 pH
R_b	0.84Ω	1.41Ω
$Z_{H,CLR}$	93Ω	93Ω
$\epsilon_{eff,H-CLR}$	2.4	2.4
α_H at 20 GHz	46 dB/m	46 dB/m

CLR model parameters. The minima of the reflection coefficient characteristics can be fitted by the model, however, a deviation over 5 dB is observed at the maxima of the reflection characteristics. A deviation of 1 dB in transmission coefficient can be quite significant in modelling of RF MEMS devices, because the emphases of RF MEMS structures are usually on their low-loss characteristics.

It should be noted here that larger bridge sizes are very important to increase the phase shift per unit length (degrees/mm), as verified with simulations considering the two cases described in Table 1. Table 3 gives the calculated degrees/dB and degrees/mm values of the two cases each of which are simulated for bridge heights of 1.2 μm and 1 μm to obtain the inserted phase shift performance. As can be concluded from Table 3, the degrees/dB performance of a loaded line phase shifter is degraded as the bridge width is increased. However, a significant improvement can be achieved in the inserted phase shift in a specific length of structure as implied with nearly 1.7–1.8 times increase in degrees/mm values at 40 and 60 GHz, which is quite important for phase shifter applications. Hence, there is a need for a new approach that can accurately model DMTL structures with larger bridge widths, which is provided in Section 4. To verify the new model with measurement results on fabricated devices, various DMTL structure are fabricated using the fabrication process explained in Section 3.

Table 3: Data for DMTL structures with dimensions in Table 1

	Case I ($w=35\ \mu\text{m}$)		Case II ($w=100\ \mu\text{m}$)	
	Frequency, GHz	40	60	40
Degrees/dB	98	120	64	74
Degrees/mm	10.9	16.8	18.4	30.6
Loss, dB	0.87	1.1	[2.2–3.8]	[3.1–5.5]
Phase, degrees	85.6	133.6	192.8	321
Unit cell length, μm	197	262		
Total length, mm	7.486	10.48		

Number of bridges for both of the structures is 40. The improvement in the values of $^\circ/\text{mm}$ shows the necessity to increase the bridge width

3 Fabrication process

The DMTL structures are fabricated using the standard process developed at METU for implementation of RF MEMS components, which is based on electroforming on a 500 μm -thick Pyrex 7740 glass substrate. Figure 4 shows the fabrication process steps. The fabrication starts with the deposition of 100/2500 \AA -thick Ti/Cu layer using sputtering in order to form the seed layer for the copper electroplating. The 2 μm -thick copper is deposited using electroplating, while a 3 μm -thick patterned photoresist is used as the mould. This process is followed by the evaporation of 0.1 μm -thick gold. The base metallisation layer is completed using a lift-off technique applied on the gold layer and selective etching of the Ti/Cu seed layer. The next step is the deposition of 0.2–0.4 μm -thick Si_3N_4 as the dielectric layer using plasma-enhanced-chemical-vapour-deposition (PECVD) process. The dielectric layer is then patterned with reactive-ion-etching (RIE) process. This dielectric layer

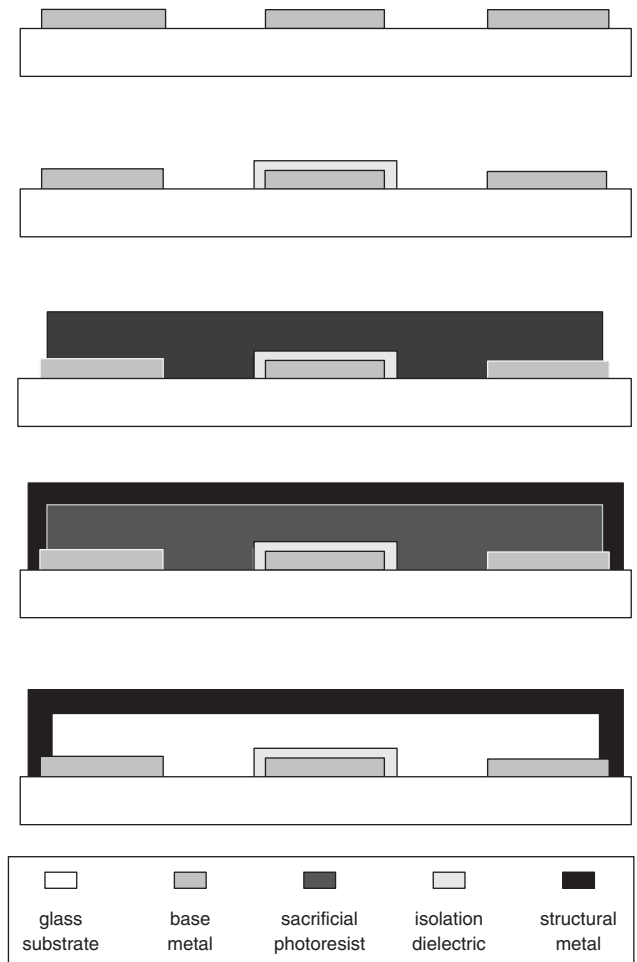


Fig. 4 Fabrication process flow

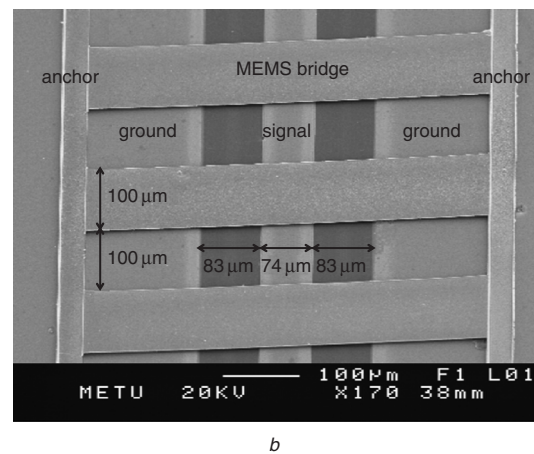
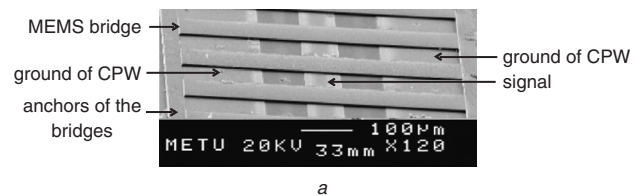


Fig. 5 SEM views of DMTL structure with interbridge spacing of 100 μm and bridge width of 100 μm

a A portion of a DMTL structure where MEMS bridges are placed periodically
b Top view of 3 cascaded MEMS bridges of the same DMTL structure

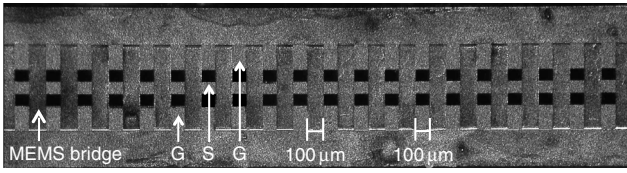


Fig. 6 Photograph of fabricated DMTL with interbridge spacing of 100 μm and bridge width of 100 μm

is deposited to avoid DC short when the MEMS bridges are collapsed with electrostatic actuation. A photoresist sacrificial layer is used between the base metal and the structural layer, which is used to realise MEMS bridges. The thickness of the photoresist can be varied between 2 μm and 5 μm depending on the DMTL type to be implemented. The pattern of the sacrificial layer is followed by the sputter-deposition of 100/2500 \AA -thick Ti/Cu layer, which is used as the seed of the structural layer electroplating. 1 μm -thick nickel is electroplated as the structural layer forming the MEMS bridges having etching holes on them defined by the mould photoresist. These holes ensure the ease of etching of the sacrificial layer and reduce the air damping of the MEMS bridges. The process is finalised with the removal of the sacrificial photoresist with stripper followed by the critical point drying. Figure 5 gives scanning electron microscope (SEM) views of a DMTL structure fabricated at METU and Fig. 6 shows a top view photograph of one of the fabricated DMTL structures. Using this process, a number of DMTL structures with different physical dimensions are fabricated to verify the new circuit model proposed in this study, which is explained below.

4 Proposed circuit model

Figure 7 shows the circuit schematics of the proposed model [7–8], where all parts of the DMTL structure, including the bridge part, are actually transmission lines having different parameters and discontinuities in between. This approach considers that the MEMS bridge is similar to a top cover of a conductor backed CPW (CBCPW) [9]. As the MEMS bridge is much closer to the signal line than the planar ground of the CPW and the back cover, most of the field would be confined between the signal line and the MEMS bridge. Considering this, the DMTL structure is modelled with three components. The first component is the CPW which converges to a microstrip (MS) line with a low impedance where the ground of the microstrip is the MEMS bridge. The second component is the high-impedance CPW, modelling the unloaded part of the DMTL. The third component LC networks are employed to account for the abrupt impedance and field distribution change in the transition regions from high to low impedance lines. The inductance in the LC network models the change in the current distribution, and the capacitance accounts for the fringe fields at the discontinuity region. The derivation of the three components of the model is presented in detail in the following subsection, which is followed

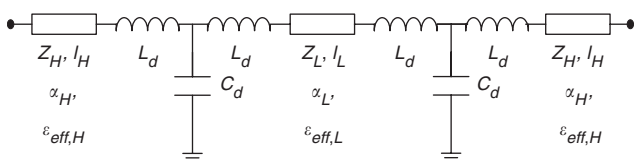


Fig. 7 Proposed circuit model for DMTL, where MEMS bridges are represented with low-impedance transmission lines [7–8]

by a subsection on the verification of low-impedance line parameters.

4.1 High-impedance line parameters

The unloaded parts of the designed DMTL structures are simply unloaded CPW with a cross-section shown in Fig. 8a, and these parts can be modelled with a high-impedance transmission line. Equations (1)–(6) provide the formulation that is used to calculate the characteristic impedance Z_H , the effective permittivity ϵ_{eff} , and the attenuation constant α_H , which is obtained by conformal mapping [9–11]:

$$\epsilon_{eff} = 1 + q(\epsilon_r - 1) \quad (1)$$

$$q = \frac{\frac{K(k_1)}{K(k'_1)}}{\frac{K(k_1)}{K(k'_1)} + \frac{K(k_2)}{K(k'_2)}} \quad (2)$$

$$k_1 = \frac{\tanh(\pi S/4H)}{\tanh[\pi(S+2W)/4H]} \quad k'_1 = \sqrt{1-k_1^2} \quad (3)$$

$$k_2 = \frac{S}{S+2W} \quad k'_2 = \sqrt{1-k_2^2} \quad (4)$$

$$Z_H = \frac{60\pi}{\sqrt{\epsilon_{eff}}} \frac{1}{\frac{K(k_1)}{K(k'_1)} + \frac{K(k_2)}{K(k'_2)}} \quad (5)$$

$$\alpha_H = \frac{8.686 \times 10^{-2} R_s \sqrt{\epsilon_{eff,H}}}{4\eta_0 S K(k_2) K(k'_2) (1-k_2^2)} \times \left[\frac{2S}{W} \left\{ \pi + \ln \left(\frac{4\pi W(1-k_2)}{t(1+k_2)} \right) \right\} + 2 \left\{ \pi + \ln \left(\frac{4\pi S(1-k_2)}{t(1+k_2)} \right) \right\} \right] \quad (6)$$

where W , S and H are the physical dimensions of the structure given in Fig. 8a, and t is the metal thickness, R_s is the surface resistance given by $R_s = \sqrt{\pi f \mu_0 / \sigma}$, σ is the conductivity of the metal, η_0 is the free-space impedance, and $K(k)$ is the complete elliptic integral of the first kind.

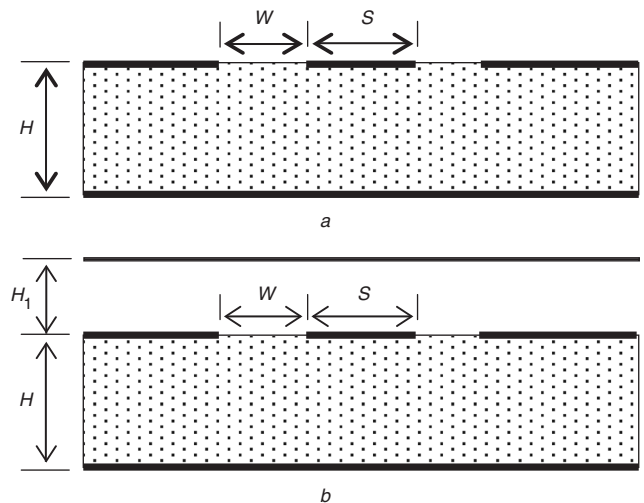


Fig. 8 Conductor-backed coplanar waveguides
a Standard
b With a top cover

The ratios K/K' can be calculated as

$$\frac{K}{K'} = \begin{cases} \frac{1}{\pi} \ln \left(2 \frac{1 + \sqrt{k_2}}{1 - \sqrt{k_2}} \right) & 0.7 \leq k \leq 1 \\ \left[\frac{1}{\pi} \ln \left(2 \frac{1 + \sqrt{k_2'}}{1 - \sqrt{k_2'}} \right) \right]^{-1} & 0 \leq k \leq 0.7 \end{cases} \quad (7)$$

Table 4 gives the dimensions and calculated parameters of the high-impedance parts of three DMTL structures denoted as cases III, IV and V, which are implemented on a 500 μm -thick Pyrex 7740 glass substrate with $\epsilon_r = 4.6$ and $\tan \delta = 0.005$. The metallisation of the CPW line forming the high-impedance part of DMTL is taken as 2 μm of copper ($\sigma \cong 5 \times 10^7 \text{ S/m}$). Figure 9 shows the measurement results on unloaded CPW of the third structure denoted as case V and its modelling to verify the accuracy of the calculated high-impedance parameters. The extracted values obtained from measurements for Z_H , $\epsilon_{\text{eff},H}$, and α_H are 70 Ω , 2.77, and 0.3 dB/cm, respectively. These values are very close to the calculated parameters presented in Table 4, where Z_H , $\epsilon_{\text{eff},H}$ and α_H are 70 Ω , 2.77 and 0.25 dB/cm, respectively. The slight deviation of the loss parameter α_H might be due to the substrate and radiation losses which are underestimated in the analytical expression. Similar observations are obtained for cases III and IV, i.e. Z_H and $\epsilon_{\text{eff},H}$ are exactly same for the measured and

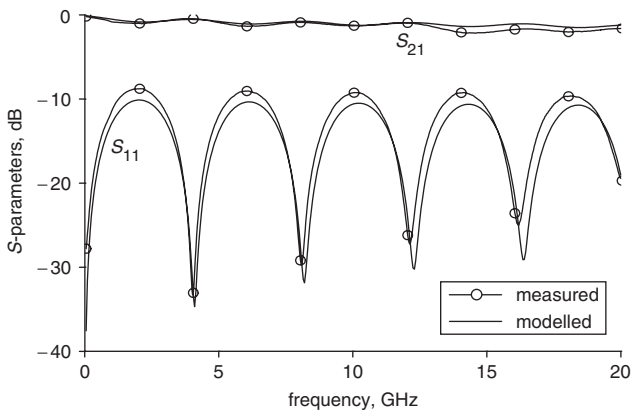


Fig. 9 Measured S -parameters for unloaded CPW line (DMTL case V) on glass substrate
High-impedance line parameters extracted from measurement results are quite close to the calculated values

calculated values, while calculated α_H is slightly lower than the measured α_H .

4.2 Low-impedance line parameters

The low-impedance line parameters (Z_L , $\epsilon_{\text{eff},L}$) are calculated considering the coplanar waveguide with a top cover formulation, where the MEMS bridge is assumed to be top cover. To complete a parametric study, the top cover height is varied as $H = 2, 3, 4$ and 5 μm . Equations (1)–(3) and (5) are also valid for this structure. Instead of (4), the following equation is used to determine k_2 as

$$k_2 = \frac{\tanh(\pi S/4H_1)}{\tanh[\pi(S+2W)/4H_1]} \quad k_2' = \sqrt{1 - k_2^2} \quad (8)$$

where H_1 is the top cover height as described in Fig. 8b. It should be noted here that the value obtained by (8) is very much close to unity, however, it should not be approximated as one, which will result in incorrect values in (1)–(3) and (5). To be more specific, up to 25 significant digits may be needed during the calculation of k_2 to obtain accurate value of k_2 . Table 5 gives the calculated parameters for low-impedance lines. The characteristic impedance Z_L and effective permittivity $\epsilon_{\text{eff},L}$ values for low-impedance transmission line can also be calculated using MS formulation, because the CPW converges to an MS line underneath the bridge, as explained previously. Z_L values calculated with MS formulation yields similar results with the ones given in Table 5. In this case, $\epsilon_{\text{eff},L}$ will simply be unity, because the airgap between the signal line of the CPW and the MEMS bridge behaves as a substrate of this MS line. There is no analytical expression available in open literature for the attenuation constants α_L of the CPW structures with a top cover at a height in the order of a few micrometres, so they are extracted from EM simulations in Ansoft HFSS v9.2, as presented in the following subsection.

4.3 Discontinuity parameters and measurements

Discontinuity parameters, i.e. inductance and capacitance values, are extracted using the simulation of DMTL structures with having only 10–14 MEMS bridges to reduce the computational time. Table 6 gives the discontinuity parameters obtained by minimising the mean square error between these EM and the circuit model in Fig. 7. Figure 10 shows the variation of the discontinuity parameters with respect to the centre conductor width and the MEMS bridge height values. The variation of the capacitance values

Table 4: Dimensions for three DMTL structures, $w = 100 \mu\text{m}$ for all structures

Type	$W, \mu\text{m}$	$G, \mu\text{m}$	$s', \mu\text{m}$	Number of bridges	Total length, mm	Z_H, Ω	$\epsilon_{\text{eff},H}$	$\alpha_H, \text{dB/cm}$
Case III	74	83	100	112	22.4	89	2.78	0.25
Case IV	96	87	200	75	22.5	83	2.78	0.23
Case V	122	59	400	45	22.5	70	2.77	0.25

Table 5: Calculated low-impedance line parameters, Z_L (Ω), α_L (dB/cm), $\epsilon_{\text{eff},L}$ at 10 GHz

Type	$h = 2 \mu\text{m}$			$h = 3 \mu\text{m}$			$h = 4 \mu\text{m}$			$h = 5 \mu\text{m}$		
	Z_L	α_L	$\epsilon_{\text{eff},L}$									
Case III	9.12	3.96	1.12	13.01	2.62	1.17	16.54	1.96	1.22	19.76	1.57	1.27
Case IV	7.17	3.99	1.1	10.31	2.64	1.14	13.21	1.97	1.19	15.89	1.58	1.23
Case V	5.68	4.02	1.09	8.2	2.66	1.13	10.54	1.99	1.18	12.72	1.59	1.22

Table 6: Fitted parameters extracted from optimisation

Type	$h = 2 \mu\text{m}$		$h = 3 \mu\text{m}$		$h = 4 \mu\text{m}$		$h = 5 \mu\text{m}$	
	L_{dr} , pH	C_{dr} , fF						
Case III	6.27	4.09	5.89	3.81	5.88	3.01	5.89	2.47
Case IV	6.47	4.91	6.09	4.36	5.47	4.10	6.39	3.15
Case V	4.03	6.97	3.38	6.07	3.27	5.13	3.88	3.98

Parameters except L_{dr} , C_{dr} and α_L are fixed during the optimisation

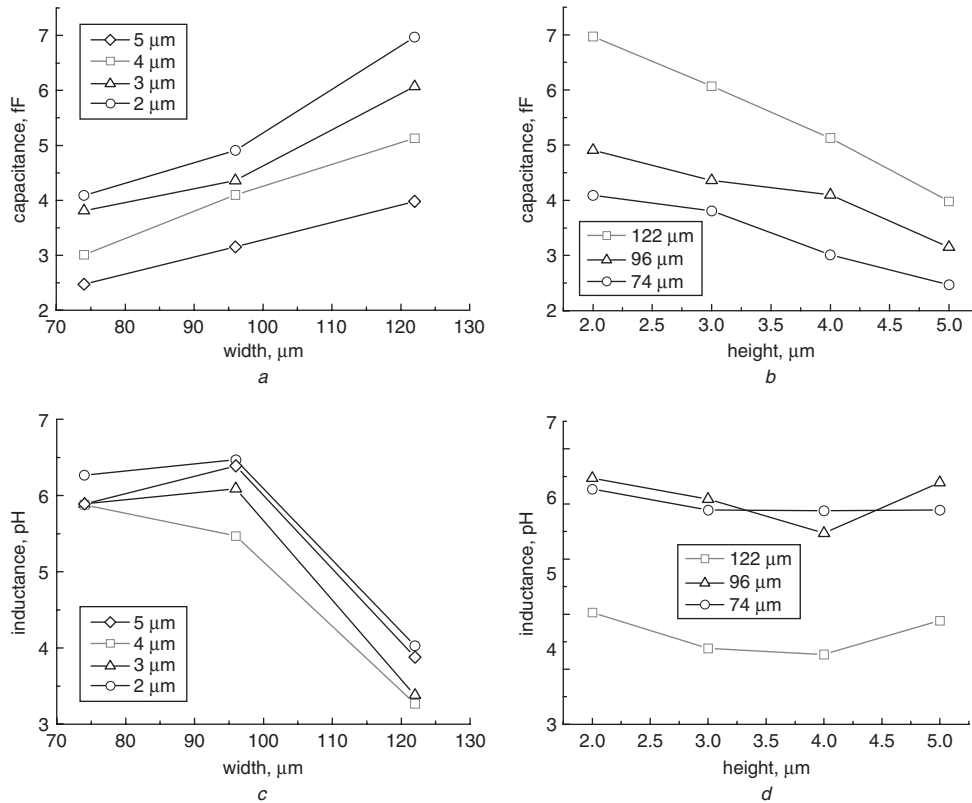


Fig. 10 Discontinuity parameter graphs for different CPW dimensions
a Discontinuity capacitance against centre conductor width
b Discontinuity capacitance against bridge height
c Discontinuity inductance against centre conductor width
d Discontinuity inductance against bridge height

in Fig. 10*a* is linear with respect to centre conductor width, which is expected as the fringe fields should increase with increasing centre conductor width. A similar linear behaviour is observed in Fig. 10*b* when the bridge height is varied, which is also expected regarding the reported fringe capacitance values [1]. The trend of the discontinuity inductance is not a strong function of bridge height, but the width of the centre conductor has direct influence on these values as seen in Figs. 10*c* and *d*. This behaviour can be explained as the current distribution is affected more significantly with the centre conductor width, but this is not valid for the bridge height.

The proposed model in Fig. 7 is verified with measurements on DMTL structures having various bridge heights. Figures 11–15 show the comparison of the measurement and the model reflection and transmission coefficients for the structures denoted as case III (for bridge height $h = 5 \mu\text{m}$), case IV (for bridge heights $h = 3$ and $5 \mu\text{m}$), case V (for bridge heights $h = 3$ and $5 \mu\text{m}$). The S -parameters of the measurement results and the model are very close for all cases except case V with $3 \mu\text{m}$ bridge

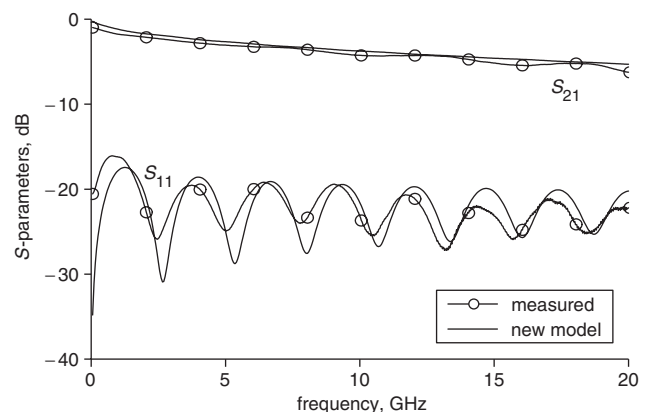


Fig. 11 Measurement results for the DMTL case III, $h = 5 \mu\text{m}$

height, where there is a slight deviation in the fitting of the model for the magnitude of the reflection coefficient; however, this deviation stems from the sacrificial layer height difference along the device, as determined with

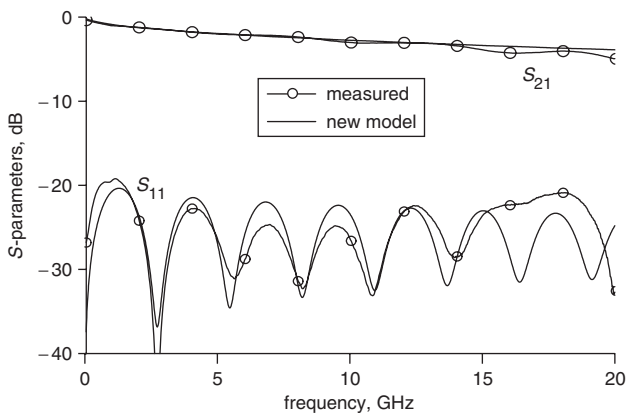


Fig. 12 Measurement results for the DMTL case IV, $h = 5 \mu\text{m}$

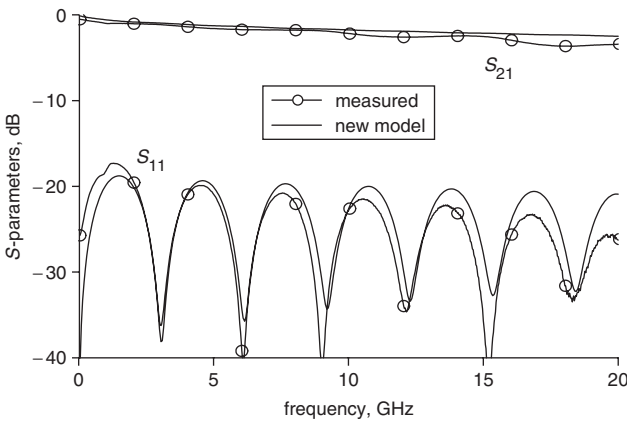


Fig. 13 Measurement results for the DMTL case V, $h = 5 \mu\text{m}$

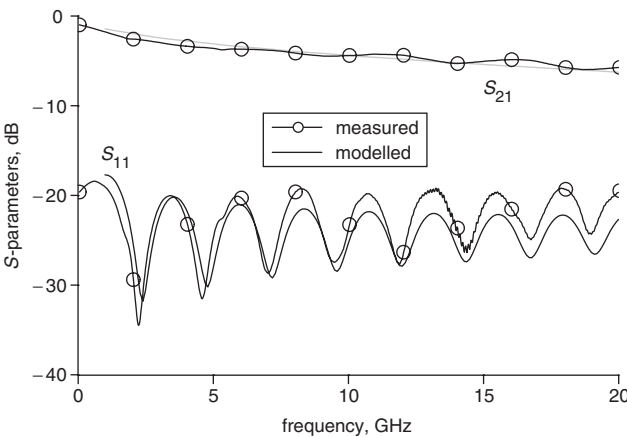


Fig. 14 Measurement results for the DMTL case IV, $h = 3 \mu\text{m}$

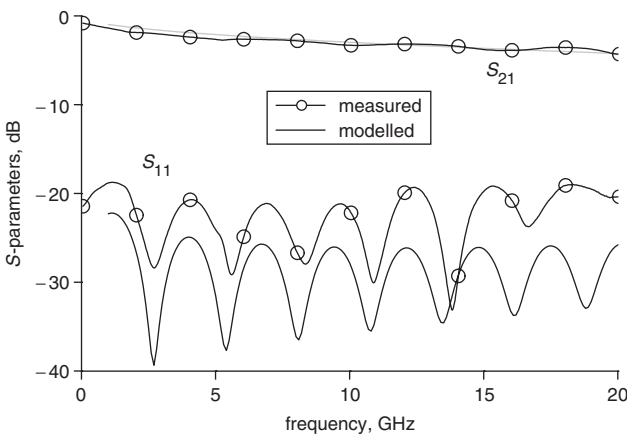


Fig. 15 Measurement results for the DMTL case V, $h = 3 \mu\text{m}$

optical surface profiler. It should be noted that the agreement between the measurement and the model is still satisfactory even for this case, when the phase of the transmission coefficient given in Fig. 16 is considered, which is crucial in phase shifter applications.

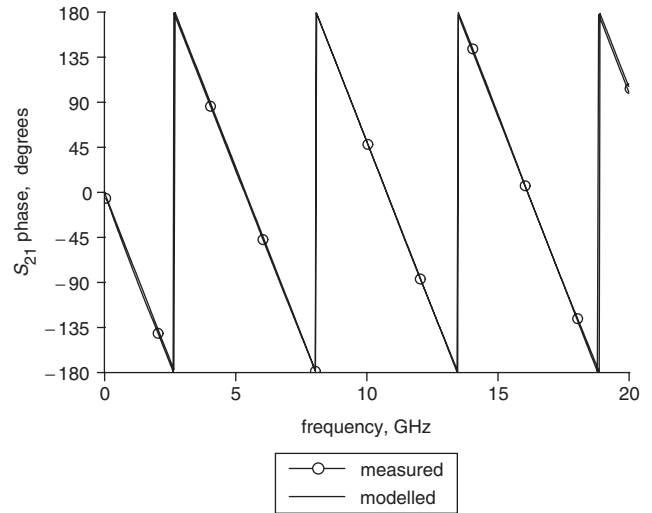


Fig. 16 Measurement and circuit model results on phase of transmission coefficient for the DMTL case V, $h = 5 \mu\text{m}$

The LC values extracted from the EM simulation results can also be compared with those extracted from the measurement results, however LC values are very sensitive to even small dimensional changes in fabrication compared to the design. The deviation of the designed and actual fabricated device dimensions is inevitable. Tables 7 and 8 give the LC values extracted from the EM simulation results and the measurement results for $h = 5 \mu\text{m}$ and $h = 3 \mu\text{m}$, respectively. The discrepancy in the results is still acceptable, considering the variations in fabricated device dimensions.

4.4 Verification of low-impedance line parameters using EM simulations

This subsection presents further verification of the low-impedance line parameters that are extracted using CPW with a top cover formulation, as this formulation has not been examined for a top cover height in the order of a few micrometres in the literature. For this purpose, the low-impedance line parameters of the DMTL structures are extracted using EM simulations and these results are compared with the parameters extracted with CPW with a top cover formulation.

Figure 17 shows the S -parameter results for a CPW with a length of 10 mm and with a top cover at $5 \mu\text{m}$ extending through all over the line, which is the expected characteristic of a transmission line. The port impedance of this simulation result is tuned to minimise the effect of the reflection coefficient and to avoid multiple reflection at the ports due to the low characteristic impedance of the line. Figure 18 shows the reflection coefficient value, which reaches its minimum value when the port impedance is tuned as 20.5Ω and the ripples on the transmission coefficient vanish. This value is equal to the characteristic impedance of the line, which is quite close to the calculated value of 19.76Ω in Table 5. The loss per unit length value, i.e. the attenuation constant, is extracted directly from the transmission coefficient because the effect of reflection loss is removed. As we repeat the simulation for different lengths of transmission lines, the length independent behaviour of

Table 7: Simulated and measured discontinuity and loss parameters of DMTL structures with a bridge height of $h = 5 \mu\text{m}$

Case	Simulated			Measured		
	L_{dr} pH	C_{dr} fF	α_L dB/cm	L_{dr} pH	C_{dr} fF	α_L dB/cm
Case III	5.89	2.47	1.57	9.59	1.61	1.85
Case IV	6.39	3.15	1.58	8.98	3.78	1.59
Case V	3.88	3.98	1.59	11.09	2.08	1.20

α_L is calculated at 10 GHz

Table 8: Simulated and measured discontinuity and loss parameters of DMTL structures with a bridge height of $h = 3 \mu\text{m}$

Case	Simulated			Measured		
	L_{dr} pH	C_{dr} fF	α_L dB/cm	L_{dr} pH	C_{dr} fF	α_L dB/cm
Case IV	6.09	4.36	2.64	7.47	7.34	2.34
Case V	3.38	6.07	2.66	9.39	5.93	1.76

α_L is calculated at 10 GHz

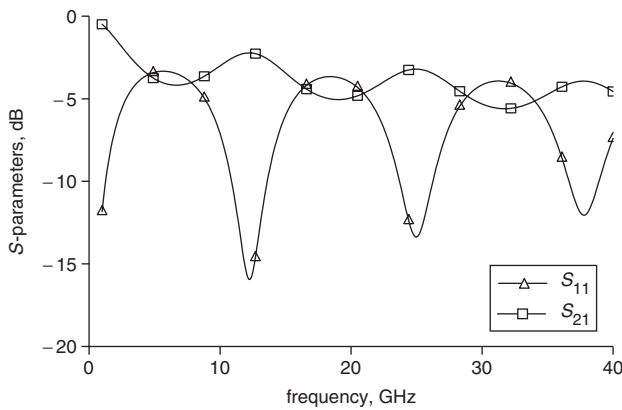


Fig. 17 S -parameter results for 10mm length of CPW with top cover at $5 \mu\text{m}$

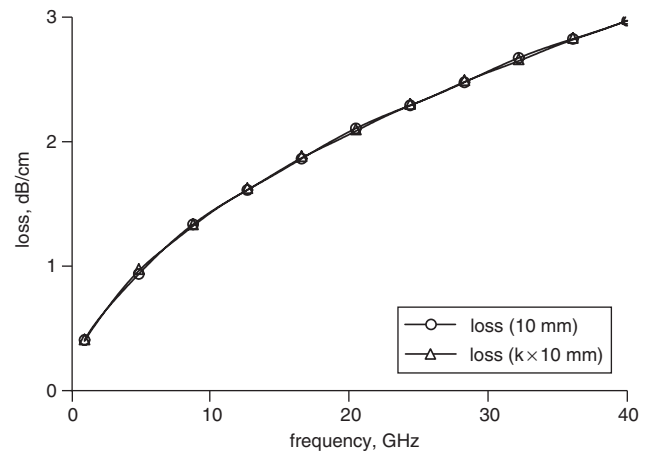


Fig. 19 Loss (dB/cm) values of CPW with top cover structures. The simulations are performed on different lengths of transmission lines and length independent behaviour of attenuation constant is observed as the effect of the reflection coefficient is removed

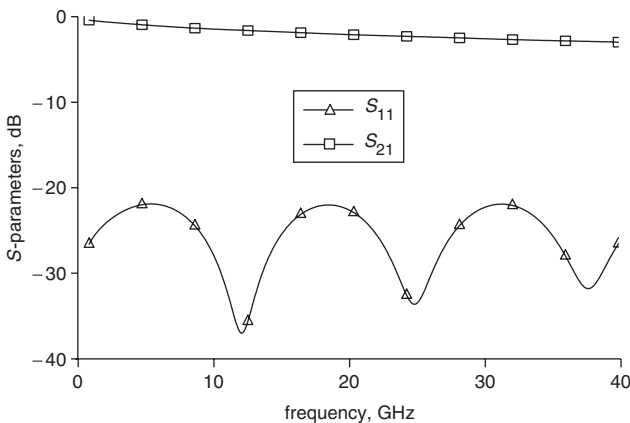


Fig. 18 S -parameter results for 10mm length of CPW with top cover at $5 \mu\text{m}$ where port impedance is tuned as 20.5Ω

the attenuation constant is observed. Figure 19 shows the extracted loss values for lines having different lengths. These loss values are also sufficiently close to the values presented in Table 5. These simulations verify that the formulation on CPW with a top cover can be used to accurately determine the low-impedance line parameters of DMTL structures. It should be noted here that the loss values increase with decreasing MEMS bridge height as given in Table 5. This observation is physically reasonable considering the field distribution of a CPW with a top cover as explained in this

Section. In this structure, the field is mostly confined between the signal line of the CPW and the top cover. This causes the current density for the loaded part to increase significantly, resulting in a considerable increase in the conductor losses. The decrease in the characteristic impedance and the effective permittivity is explained with the increase of per-unit-length capacitance and the amount of field propagating through the airgap.

5 Comparison between CLR model and proposed model

To make a comparison between the CLR model and the proposed model, the DMTL structures described in Table 1 are also examined with the new model, where C_{dr} , L_d and α_L are considered as free variables. Figures 20 and 21 show the results for case I and II modelled with the proposed approach and the CLR approach. Table 9 gives the results of the optimisation on the free variables of the new model. The loss of the low-impedance transmission lines is lower than the extracted loss values as explained in Section 4.4, which can be due to the numerical accuracy of the HFSS simulations. The CLR model is successful in estimating both reflection and transmission characteristics of case I, as can be seen in Fig. 20. The proposed model can also

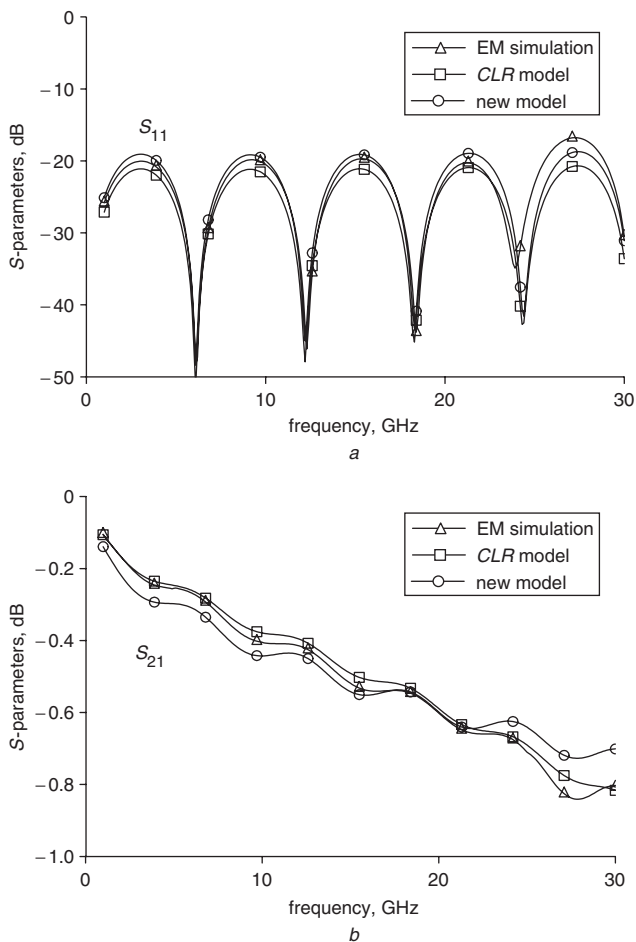


Fig. 20 Comparison of proposed model with CLR model in modelling EM simulation of DMTL structure with 35 μm bridge width
 a Reflection characteristics
 b Transmission characteristics
 Both of the models provide satisfactory agreement with EM simulation

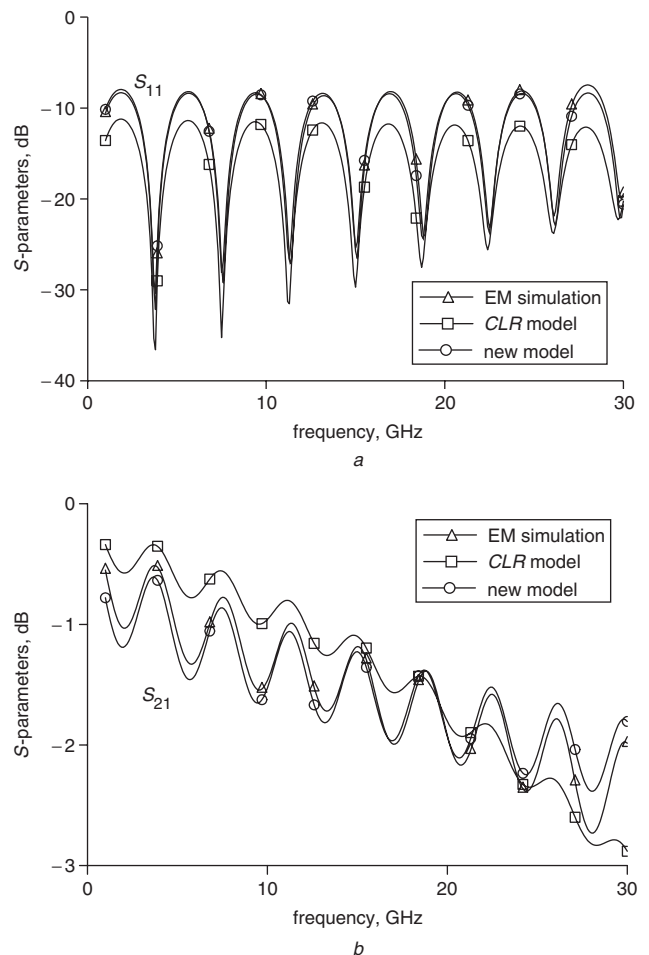


Fig. 21 Comparison of proposed model with CLR model in modelling EM simulation of DMTL structure with 100 μm bridge width
 a Reflection characteristics
 b Transmission characteristics
 The CLR model shows significant deviations with the EM simulations because the bridge part cannot be modelled as a lumped element due to its increased electrical length

provide acceptable agreement for estimating the characteristics of case I. However, the CLR model can express the loss dependency of \sqrt{f} better than the proposed model, because the loss of the structure is dominated by the loss of the unloaded CPW that changes with \sqrt{f} due to the skin effect as expressed in (6). However, for case II, the deviation between the CLR model and EM simulation results can clearly be observed especially when the transmission coefficient in Fig. 21b is examined. The proposed model can provide a very good agreement for both reflection and transmission coefficient characteristics. The loss of the structure shows properties of a transmission line because the loaded part of the structure behaves as a transmission line due to its increased length to 100 μm . The resistance R which models the bridge losses in the CLR model, causes a deviation in modelling the DMTL structure with increased bridge width. Hence, it is clear from this example that the CLR model cannot provide a satisfactory result for DMTL structures with electrically long bridge width values, while they can be accurately modelled with the new modelling approach proposed in this study.

The proposed model and the CLR approach can also be compared in terms of estimating the Bragg frequency of the DMTL structures, which is a phenomenon related to the approach of guided wavelength to the periodic spacing

Table 9: Extracted parameters of proposed model for DMTL structures with dimensions in Table 1

Parameter	Case I	Case II
Z_H	93 Ω	93 Ω
$\epsilon_{\text{eff},H}$	2.4	2.4
α_H	0.3 dB/cm	0.3 dB/cm
L_d	3.24 pH	6.58 pH
C_d	4.22 fF	8.54 fF
Z_L	4.3 Ω	4.3 Ω
$\epsilon_{\text{eff},L}$	1.1	1.1
α_L	0.2 dB/cm	0.49 dB/cm

of discrete components [12]. Figure 22 shows the frequency sweep for both of the models, in order to observe the Bragg frequency for DMTL structures. According to both models, the structure with 35 μm bridge width (case I) has a Bragg frequency of approximately 175 GHz when the bridge inductance in the CLR model is 0 pH. For the second structure (case II) having a bridge width of 100 μm , the Bragg frequency for both models is found to be at

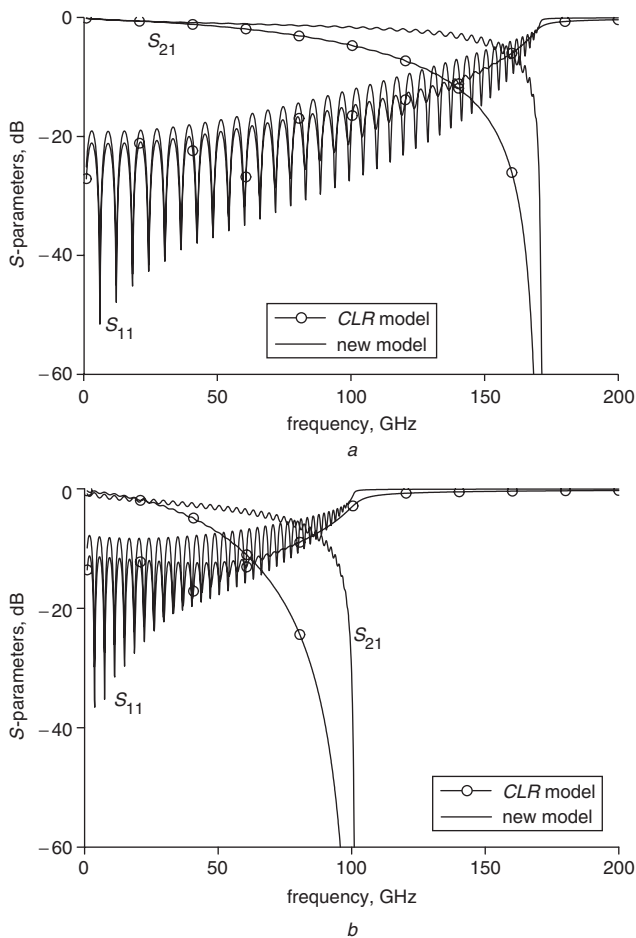


Fig. 22 Frequency sweep for both of the models in order to observe the Bragg frequency for DMTL structures investigated to test the performance of the models
 Bridge inductance in the CLR model is taken as 0 pH
 a Case I
 b Case II
 Both of the models give nearly the same Bragg frequency values

approximately 102 GHz again for 0 pH bridge inductance in the CLR model verifying that both models estimate nearly the same Bragg frequencies. The reduction in the Bragg frequency from 175 GHz to 102 GHz is also expected because the periodic spacing of the MEMS bridges is increased from 197 μm to 262 μm . In the second analysis about Bragg frequency, the bridge inductance in the CLR model is increased to 20 pH [2], which has nearly no effect in the frequency of interest, i.e. 1–20 GHz. However, it shows its significance in the determination of the Bragg frequency: the Bragg frequency shifts from 175 GHz to 129 GHz for case I and 102 GHz to 88 GHz for case II. Moreover, as can be seen from Figs. 23a and 23b, the depths of the ripples do not follow the same pattern in the results of two models, as the frequency approaches the vicinity of the Bragg frequency. The effect of the bridge inductance is quite significant for the structures with lower interbridge spacing, which is 197 μm for case I. The shift in the Bragg frequency is from 175 GHz to 129 GHz, i.e. about 46 GHz, with the insertion of 20 pH bridge inductance to the model, whereas it is from 102 GHz to 88 GHz, i.e. about 14 GHz, for the structure having an increased interbridge spacing of 262 μm . The Bragg frequencies of these structures were also observed with EM simulations. The Bragg frequency is found to be at 130 GHz for case I and at 90 GHz for case II, which are quite close to the results of the CLR model with 20 pH of bridge inductance is employed.

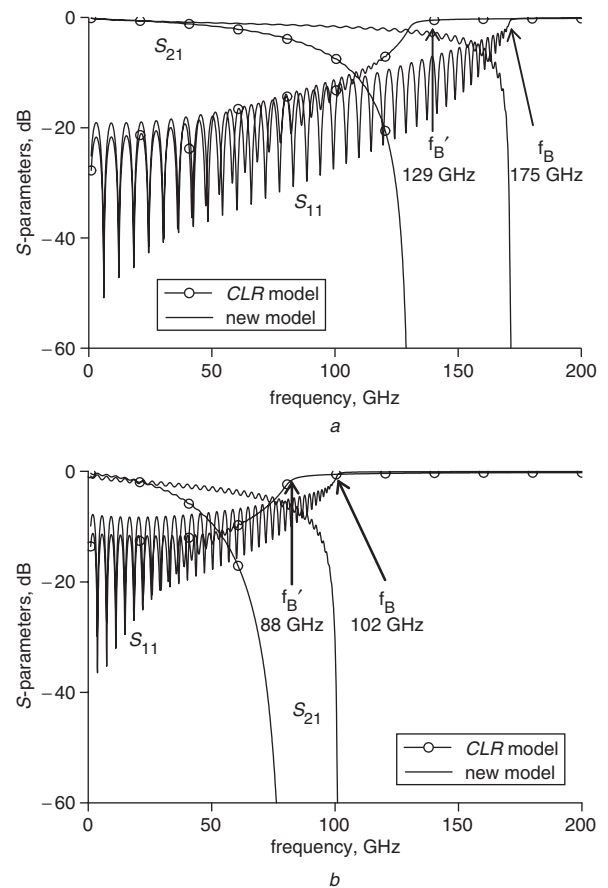


Fig. 23 Frequency sweep for both of the models in order to observe the Bragg frequency for DMTL structures investigated to test the performance of the models
 Bridge inductance in the CLR model is taken as 20 pH
 a Case I
 b Case II
 The inductance in the CLR model shows its significance in the determination of the Bragg frequency and this model gives closer results for the Bragg frequency values found by EM simulations

6 Conclusion

This paper has presented a new model for DMTL structures, its parametric study and a comparison between the CLR model and the new model. The proposed new model consists of a high-impedance transmission line for the unloaded CPW, low-impedance transmission line for the MEMS bridge and LC networks for the transitions. The accuracy of the model is verified with simulations and measurements on different DMTL structures with different physical dimensions that are fabricated with an RF MEMS process based on electroforming on a glass substrate. The simulated and fabricated structures include DMTL structures with various MEMS bridge heights (2, 3, 4 and 5 μm) and centre conductor widths (74, 96 and 122 μm). These structures are accurately modelled with the new approach, when both EM simulation results and measurement results are considered. The discontinuity parameters L_d and C_d extracted using EM simulations, show a slight deviation compared to those extracted using measurement results, due to possible variations in designed and fabricated device dimensions. The new model can accurately be used not only for DMTL structures with moderate bridge widths (such as 35 μm), but also for DMTL structures with large bridge widths (such as 100 μm), which is necessary for phase shifter applications, in order to increase the phase shift per unit length (degrees/mm) value. It is also shown that DMTL

structures with large bridge widths cannot be modelled accurately with the conventional *CLR* approach, justifying the new modelling approach proposed in this study.

7 Acknowledgments

This research is supported by The Scientific and Technical Research Council of Turkey (TUBITAK-EEEAG-101E023 and 102E036), Turkish State Planning Organization (DPT), and AMICOM (Advanced MEMS For RF and Millimeter Wave Communications) Network of Excellence under the 6th Framework Program of the European Union. The authors also would like to thank to METU-MET staff for their support in the fabrication and to Orhan Sevket Akar for process development and packaging.

8 References

- 1 Rebeiz, G.M.: 'RF MEMS theory, design, and technology' (John Wiley & Sons, Hoboken, NJ, 2003)
- 2 Barker, N.S., and Rebeiz, G.M.: 'Optimization of distributed MEMS transmission-line phase shifters – U-band and W-band designs', *IEEE Trans. Microw. Theory Tech.*, 2000, **48**, pp. 1957–1966
- 3 Barker, N.S., and Rebeiz, G.M.: 'Distributed MEMS true-time delay phase shifters and wide-band switches', *IEEE Trans. Microw. Theory Tech.*, 1998, **46**, pp. 1881–1890
- 4 Borgioli, A., Liu, Y., Nagra, A.S., and York, R.A.: 'Low-loss distributed MEMS phase shifter', *IEEE Microw. Guid. Wave Lett.*, 2000, **10**, pp. 7–9
- 5 Muldavin, J.B., and Rebeiz, G.M.: 'X-band tunable MEMS resonators'. Topical Meeting on Silicon Monolithic Integrated Circuits in RF Systems, 2000, pp. 116–118
- 6 Lakshminarayanan, B., and Weller, T.: 'Tunable bandpass filter using distributed MEMS transmission line', *IEEE MTT-S Int. Microw. Symp. Dig.*, 2003, **3**, pp. 1789–1792
- 7 Topalli, K., Unlu, M., Sagkol, H., Demir, S., Aydin Civi, O., Koc, S., and Akin, T.: 'A new model for distributed MEMS transmission line'. Proc. IEEE Int. Antennas Propag. Symp., Monterey, CA, June 2004, pp. 2855–2858
- 8 Unlu, M., Topalli, K., Demir, S., Aydin Civi, O., Koc, S., and Akin, T.: 'A parametric modelling study on distributed MEMS transmission lines'. Proc. 34th European Microw. Conf., Amsterdam, The Netherlands., October 2004, pp. 1157–1160
- 9 Simons, R.N.: 'Coplanar waveguide circuits, components and systems' (John Wiley & Sons, New York, 2001)
- 10 Gupta, K.C., Garg, R., Bahl, I., and Bhartia, P.: 'Microstrip lines and slotlines' (Artech House, Norwood, MA, 1996, 2nd edn.)
- 11 Hoffmann, R.K.: 'Handbook of microwave integrated circuits' (Artech House, Norwood, MA, 1987)
- 12 Saleh, B.A., and Teich, M.C.: 'Fundamental of photonics' (John Wiley & Sons, New York, 1991)